NUMERICAL AND EXPERIMENTAL INVESTIGATION OF A TURBINE GUIDE VANE WITH CONJUGATE HEAT TRANSFER METHOD

by

Youhong LIU, Yifu LUO*, Yulin DING, Jia GUO, and Changgeng XIAO

National Key Laboratorz of Science and Technology on Aero-Thermodynamics,
School of Energy and Power Engineering, Beihang University, Beijing, China

Original scientific paper
https://doi.org/10.2298/TSCI210820024L

Three-dimensional steady-state conjugate heat transfer numerical method was utilized to study the flow and heat transfer characteristics of a turbine guide vane. In experiment, a real-sized turbine vane model and corresponding test section were designed. We verified the simulation accuracy of different turbulence models, coupling with transition model and limiter factor in conjugate heat transfer method. Compared with the experimental results, the results indicated that the SST model shows better accuracy and economy than other models studied in this paper.

Key words*: turbine guide vane, aerodynamic parameters, heat flux sensor, heat transfer, turbulence models*

Introduction

Gas turbines are widely used in military industry and civil power generation. With the improvement of industry technology, the turbine inlet temperature continues to rise. The [1] showed that for every 56 K increase in turbine inlet temperature, the gas turbine output work is increased by 8~13%. The gas turbine is still a power source in aeronautical industry. In aeroengine, to improve the thrust-weight ratio and thermal efficiency, the key point is to increase the temperature at the turbine inlet [2]. In the future, the temperature at the turbine inlet of an aeroengine will be much higher than the current level. This undoubtedly proposes new challenges to the thermal protection in aeroengine. Over the past few decades, the temperature at the turbine inlet increased 20 K per year. However, the temperature limit of the turbine material only increased 8 K per year [3].

Turbine surface heat transfer was strongly influenced by several complex and interactive mechanisms [4]. Arts *et al*. [5] studied the effect of exit Mach number, Reynolds number, mainstream turbul, and incidence angle on the heat transfer. The thermal resistances were painted at middle plane to measure local heat flux. Graziani *et al*. [6] studied the influence of passage vortex on the heat transfer on endwall and in certain regions of the airfoil surface. Graziani *et al*. [6] indicated that the size of passage vortex, which based on the inlet boundary-layers thickness, was instrumental in determining the overall passage pressure distribution. Lang *et al*. [7], Giess *et al*. [8] made extensive measurements on the 3-D velocity field for a

*Corresponding author, e-mail: luoyifu@buaa.edu.cn

rotating turbine cascade. Testing on a real-sized engine is time-consuming and labor-intensive. A linear cascade, with fewer blades than a full annular cascade, provided better spatial resolution for the same overall flow rate [9]. Cascade with only one or two cascade channels could reduce the required flow rate and satisfied the test requirements. Ganzert *et al*. [10] conducted heat transfer measurements in a two-passage three-blade test wind tunnel. Buck *et al*. [11] studied film cooling effectiveness in a single passage test model. Two bleed slots were used to remove the boundary-layers upstream of the suction and pressure side walls. Radomsky *et al*. [12] studied a scaled-up stator turbine vane and a double-passage test section consisted of a single full vane and two half-vanes. Kodzwa [13] indicated that the design of bleed slot was redundancy. It leaded to serious difficulties in comparing numerical simulation to experiments [14].

Comparing to experiments, CFD is easier and less expensive. The CFD techniques are now sufficiently robust to use in both analysis and design for aeroengine components. With the development of computer technology, it becomes a reality to use the conjugate heat transfer (CHT) method to solve the coupled fluid-solid domain simultaneously in each iteration. The CHT method was utilized by many researchers [15, 16] in the solution of heat transfer of the turbine. The effect of laminar-turbulent transition [17] and stagnation point anomaly [18, 19] were two of concerned areas in gas turbine investigation. On the turbine surface, the transition has great influence on the flow and heat transfer. To solve the problem of inaccurate prediction for transition, Menter *et al*. [20] and Langtry *et al*. [21] proposed γ-θ transition model and coupled it with turbulence models. A series of empirical relations were used in the γ-θ transition model. For stagnation point anomaly, Kato [22] proposed limiter factor to reduce the effect of excessive turbulence production in stagnation regions.

The present work is motivated by the following requirements. The prediction accuracy of different turbulence models has been tested in simple simulation, but rarely in CHT simulation. In previous studies [23], the heat flux on the turbine surface is calculated by the temperature boundary condition, without directly measuring the heat flux on the turbine surface. Detailed entire turbine guide vane experiment is required to assess the application of different turbulence models in real-sized turbine geometry. In this study, a double-passage three-vane turbine cascade is designed. The set-up of the experimental apparatus is discussed in detail. In the measurement of heat transfer, direct measurement using heat flux sensor is utilized to reduce the error caused by indirect measurement. The experimental results are utilized to compare with and verify simulation method. Several commonly used turbulence models (with γ-θ transition model and limiter factor) are tested in this comparison. All simulations are conducted in CHT method.

Experimental apparatus

In the following sections, the experimental wind tunnel and test section are described in detail. Those methods of flow and thermal measurements are presented, and the corresponding uncertainty analysis is discussed at last.

Description of experimental tunnel

Figure 1 shows a schematic of an open-loop wind tunnel configuration. The flow is pressurized by a compressor outside test room, which could provide maximum pressure up to 8 atmosphere. The air filter is installed downstream of the compressor to purify dusty gas and condense moisture of air. Then compressed gas is stored in a gas tank to maintain stable pressure. In order to adjust mainstream pressure for experimental conditions, a reducing valve is installed upstream of test section. Before the gas-flow into the test section, it is heated by an

electric heater, and the heating power is 20000 W. The electric heater is controlled by a digital thyristor regulator. Before the gas-flows into the test section, it first passes through a steady-section. Honeycomb and damping net are installed in it to make incoming flow uniform. To adjust exit pressure, a back pressure valve is installed at the outlet of wind tunnel. Also, a silencer is installed at outlet to reduce noise pollution.

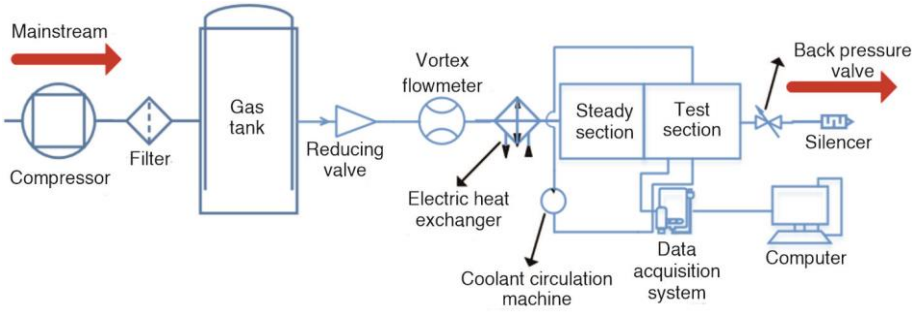

Figure 1. Schematic diagram of the test wind tunnel

An independence cooling circulation system including coolant circulation machine is designed to cool cascade test vane. The coolant is a mixture of water and alcohol to prevent the liquid from solidifying at low temperature. The temperature signals are first transferred by a data acquisition system (ADAM4018) and then recorded in the computer. The heat flux signals are recorded by a multimeter (ESCORT 3146A). The pressure data is measured by pressure sensor (0~0.6 MPa, ±0.5%) and differential pressure sensor (0~150 KPa, ±0.075%).

Description of test section

A diagram of the cascade test section including important features is presented in fig. 2. All the lengths in fig. 2 are normalized with vane chord length *C*. Four static pressure taps are installed upstream of the cascade leading edge. Two total pressure probes and two total tem-

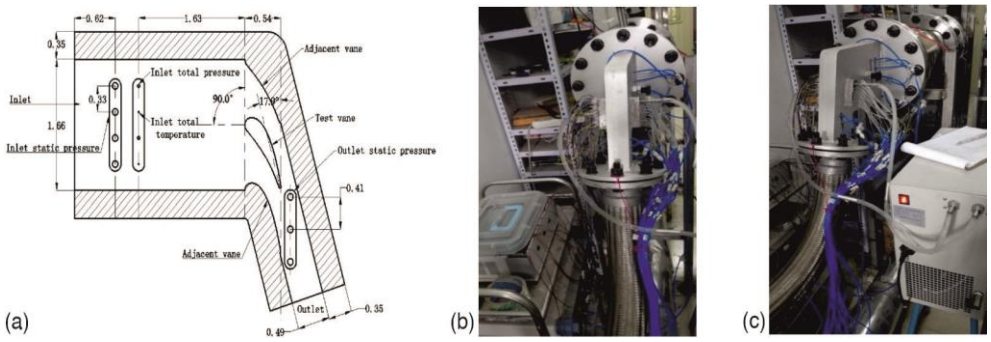

Figure 2. Schematic diagram of the test section; (a) design plan of test section, (b) test section perspective 1, and (c) test section perspective 2

perature probes are also placed and fixed alternatively upstream of the cascade leading edge. Linear cascade includes an entire test vane and two adjacent vanes only remaining half airfoil structures. The cascade pitch and vane size are all designed according to real size without scaling factor. Other three static pressure taps are positioned downstream of the cascade trailing edge. The inlet and exit airflow angles are 90° and 17.9°, respectively. Detailed key structural parameters are shown in tab. 1.

Table 1. Structural parameters of the test section

Parameters	Values
Test section inlet height, mm	20.0
Test section inlet width, mm	137.8
Test section outlet width, mm	40.5
Inlet flow angle □, °	90.0
Outlet flow angle □, °	17.9

Turbine guide vane description

The detail of test turbine vane structure is shown in fig. 3. Turbine vane surface pressure data is obtained with static pressure taps located on the turbine suction and pressure surfaces. We use laser additive manufacturing technology to print static pressure taps to the turbine surface. Each tap is perpendicular to the local vane surface and the diameter is 0.8 mm. There are 9 taps on pressure side and 12 taps on suction side.

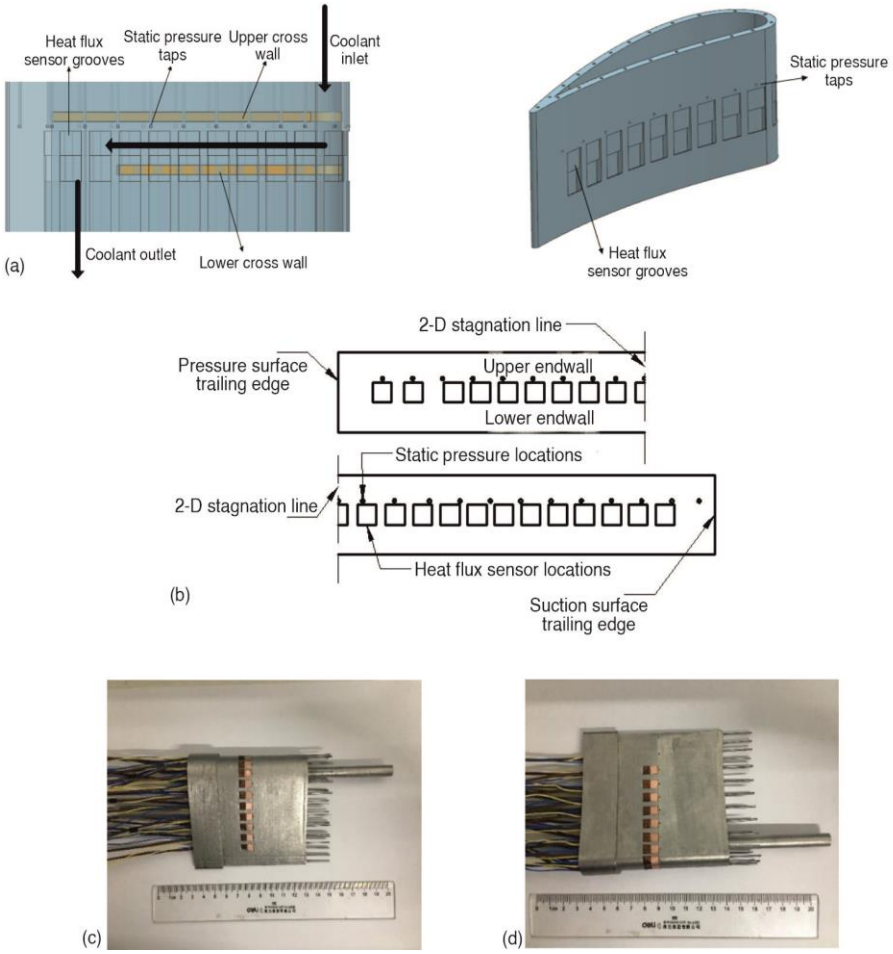

Figure 3. Detail of test turbine vane structure; (a) schematic of internal cooling channel and coolant flow, (b) diagram of turbine vane instrumentation, (c) local amplification of suction surface, and (d) local amplification of pressure surface

Two cross walls are installed inside the turbine vane to form a cooling channel, fig. 3(a). Previous in-house test results indicated that the turbine vane with cross walls has better accuracy in heat flux measurement near trailing edge than turbine vane without cross walls. Local heat flux on turbine vane surface is measured by thin film heat flux sensors. The 22 heat flux sensor grooves are fabricated on turbine vane surface. The 22 heat flux sensors are located in these grooves. The location of each sensor could be found in fig. 3(b). Surface temperatures are monitored by 22 copper-constantan thermocouples (±0.1 K) welded in the middle of the heat flux sensor. In this test, alcohol is adopted as coolant work substance. Coolant inlet temperature is 277 K, which is monitored by copper-constantan thermocouples (±0.1 K) and adjusted by a proportion integration differentiation system (±1 K). Coolant volumetric flow rate and inlet gauge pressure are 15 L per minute and 0.01 MPa, respectively. Detailed key parameters of test turbine vane are shown in tab. 2.

Table 2. Structure parameters of turbine vane

Parameters	Value
Chord length, *C*, [mm]	*C*
Pressure surface arc length,[mm]	0.97*C*
Suction surface arc length, [mm]	1.19*C*
Heat flux sensor groove depth, [mm]	0.5
Heat flux sensor groove width, [mm]	5.1
Static pressure hole diameter, [mm]	0.8
Distance between the two cross walls, [mm]	9.0

Heat transfer measurement

Present experiment uses the thin film heat flux sensor to measure surface normal heat flux and the thermocouple to measure the surface temperature. Figure 4 describes schematic of thin film heat flux sensor in detail. In fig. 4(a), each heat flux sensor consists of three layers. Resistance layer is sandwiched between two thermopile layers. In fig. 4(b), the heat flux sensor includes wiring region and sensory region. The center of the sensory region of heat flux sensor coincides with the middle plane of the vane. Copper-constantan thermocouple is welded in the middle of heat flux sensor to measure the vane surface temperature. The size of an entire sensor is 10 mm long and 5 mm wide. The size of sensory region is 5 mm long and 5 mm wide.

The local heat transfer coefficient (HTC) h [$Wm^{-2}K^{-1}$] is defined:

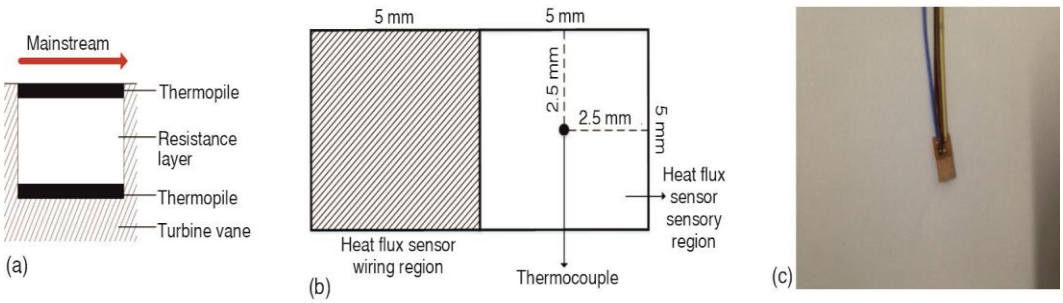

Figure 4. Schematic of thin film heat flux sensor; (a) section view of thin film flux, (b) the location of thermocouple, and (c) physical thin film heat flux sensor

$$h = \frac{q}{T_{\text{in}}^* - T_w} \tag{1}$$

where T_{in}^* [K] is the total temperature at cascade channel inlet and measured by inlet total temperature probes, T_w [K] – the local wall temperature, and q [Wm^{-2}] – the normal heat flux from mainstream to turbine solid. The heat flux, q, is measured by thin film heat flux sensor, and q can be expressed by equation:

$$q = \frac{\lambda E}{e_0 n \Delta x} \tag{2}$$

where λ [Wm^{-1}K^{-1}] is the conductivity of resistance layer, E [V] – the temperature difference electromotive force between two thermopile layers, e_0 [VK^{-1}] – the thermocouple coefficient, n [–] – the number of thermocouples in a thermopile layer, and Δx [m] – the resistance layer thickness. It could be found that the λ, e_0, n, and Δx are physical property parameters only relevant to the sensor itself. So, the eq. (2) can be simplified:

$$q = \frac{E}{\delta} \tag{3}$$

where δ [Vm^{2}W^{-1}] is the sensitivity coefficient. The sensitivity coefficient of each heat flux sensor is already calibrated before the test.

Uncertainty analysis

The uncertainty analysis in the test is based on the method in [24]. The uncertainty of measurement of each parameter by this method can be calculated by:

$$\frac{\Delta \text{Re}_c}{\text{Re}_c} = \frac{\Delta \dot{m}}{\dot{m}} \tag{4}$$

$$\frac{\Delta h}{h} = \sqrt{\frac{\Delta q^2}{q} + \frac{\Delta T_{\text{in}}^{*2} + \Delta T_w^2}{(T_{\text{in}}^* - T_w)^2}} \tag{5}$$

$$\frac{\Delta q}{q} = \sqrt{\left(\frac{\Delta E}{E}\right)^2 + \left(\frac{\Delta \delta}{\delta}\right)^2} \tag{6}$$

where Re_c [–] is the Reynolds number ($\rho U_\infty C/\mu$) based on vane chord length C, ρ [kgm^{-3}] – the air density, μ [Pa s] – the air dynamic viscosity, U_∞ [ms^{-1}] – the mainstream velocity, and $\dot{m}$ [kgs^{-1}] – the mainstream mass-flow rate.

The uncertainty of the Re_c comes from the measurement error of the mass-flow rate $\dot{m}$. From eqs. (5) and (6), the uncertainty of the convection HTC, h, comes from the heat flux measurement error and the temperature measurement error. The maximum uncertainty of the Reynolds number is 1.5%. The maximum uncertainty of the convection HTC is 7.03%.

Numerical method

For numerical solution of the flow equation, we have employed a commercial software package, ANSYS CFX. The ANSYS CFX is an implicit finite volume solver absorbing the numerical accuracy of finite element method. In CHT analysis, the temperature fields of the solid and fluid domains are solved simultaneously, calculating convection, eq. (7), in fluid domain and conduction, eq. (8), in solid domain:

$$\rho C_P\left(\frac{\partial T}{\partial t}+u\frac{\partial T}{\partial x}+v\frac{\partial T}{\partial y}+w\frac{\partial T}{\partial z}\right)=\lambda\nabla^2 T+\Phi \tag{7}$$

$$\frac{\partial T}{\partial t}=\alpha\nabla^2 T \tag{8}$$

where C_p [Jkg^{-1}K^{-1}] is the heat capacity at constant pressure, λ [Wm^{-1}K^{-1}] – the coefficient of thermal conductivity, Φ – the generalized source term, and α [m^{2}s^{-1}] – the thermal diffusivity. This paper adopts γ-θ transition model. In transition solution, two extra transport equations have been solved, one for the intermittency γ and one for the transition onset criteria terms of momentum thickness Reynolds number θ. The transport equations [20, 21] for the γ and θ are:

$$\frac{\partial(\rho\gamma)}{\partial t}+\frac{\partial(\rho U_j\gamma)}{\partial x_j}=P_{\gamma 1}-E_{\gamma 1}+P_{\gamma 2}-E_{\gamma 2}+\frac{\partial}{\partial x_j}\left[\left(\mu+\frac{\mu_t}{\sigma_\gamma}\right)\frac{\partial\gamma}{\partial x_j}\right] \tag{9}$$

$$\frac{\partial(\rho\theta)}{\partial t}+\frac{\partial(\rho U_j\theta)}{\partial x_j}=P_\theta-\frac{\partial}{\partial x_j}\left[\sigma_\theta(\mu+\mu_t)\frac{\partial\theta}{\partial x_j}\right] \tag{10}$$

Numerical mesh

The 3-D simulation model of test section including internal cooling channel is built. The numerical mesh is generated by a business software, ANSYS ICEM. As shown in fig. 5, the computational domain grid is divided into three domains: the mainstream channel, the test vane solid, and the coolant channel. We have adopted domain interface between solid and fluid to keep the heat flux conserved at the interface. The approach of connection between different domains is general grid interface method. All domains are meshed with tetrahedron mixed unstructured grid. Hexahedron grid is used to encrypt the boundary-layers grid on the solid domain surface. The maximum value of y^+ for the nearest grid point to the vane solid is around 1. The height ratio of boundary-layers increasing normal to the wall surface is 1.3 and the number of boundary-layers is 10. There are total 5.8 million elements in computational domain, including 4.4 million elements in mainstream channel, 0.8 million elements in coolant channel, and 0.6 million elements in vane solid.

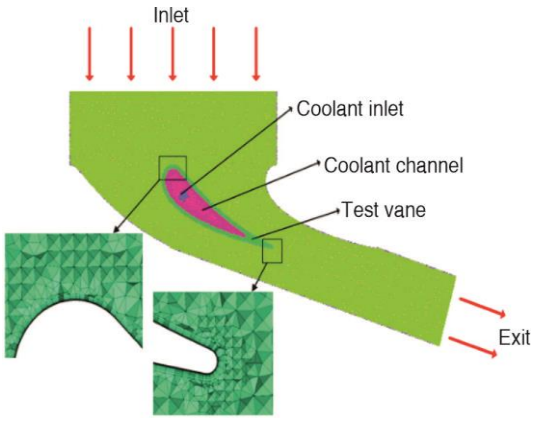

Figure 5. Schematic diagram of mesh division

Three different mesh strategies defined as coarse mesh, medium mesh and fine mesh, which have 3.8, 5.8, and 8.9 million grid elements, respectively, are chosen to validate the grid independence. The temperature and pressure distributions on middle plane of the vane in a test case for three different meshes are shown in fig. 6. Notice that the difference for pressure and temperature distributions among the results are both less than 1%. Therefore, the grid independence is assured, and the medium mesh can meet the requirements in the following simulation.

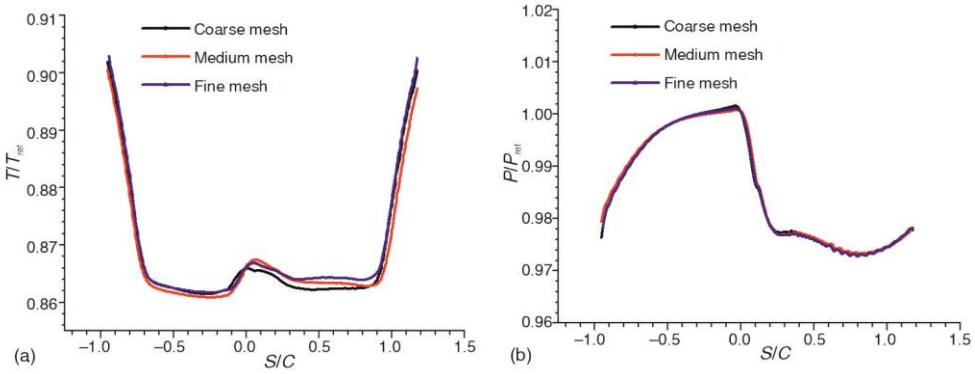

Figure 6. Distributions of pressure and temperature on middle plane of the vane; (a) pressure distributions and (b) temperature distributions

Boundary condition and turbulence model

The mainstream and the coolant channel are defined as fluid domain. The thermal conductivity as well as viscosity are modeled by the Sutherland's law. The turbine vane is defined as solid domain. Total pressure, total temperature and turbulence intensity are set at the cascade inlet coinciding with the experimental conditions. The mass-flow rate is set at the cascade outlet. At the inlet of the coolant channel domain, the total pressure is set to 0.01 MPa. The turbulence intensity is set to 5%. The cooling channel inlet temperature is set to 277 K and cooling medium flow is set to 0.25 kg/s.

In coolant channel domain, the standard k-ε turbulence model with scalable wall function is utilized. In mainstream domain, standard k-ε model, k-ω model, SST k-ω model, SST k-ω model coupling with γ-θ transition model, and SST k-ω model coupling with limiter factor are utilized. The advection scheme and turbulence numeric are both dispersed in high resolution. The convergence criteria the maximum value of each residual less than 0.000001 and the conservation target less than 0.01. Initial results are used to speed up simulation convergence.

Results and discussions

In order to verify the accuracy of different turbulence models, all the models are first verified with experimental results. The surface pressure distributions are not strongly affected by the choice of turbulence model. To avoid clutter, fig. 7 only shows numerical results of standard k-ε model and SST k-ω model. At the leading edge of the vane, due to flow stagnation, the surface static pressure is approximately equal to the total pressure. On the pressure side, surface pressure decreases slightly (from S/C = 0 to S/C = –0.55) and then drops sharply (from S/C = –0.55 to trailing edge). It indicates that gas on the pressure surface continues to accelerate. On the suction side, the surface pressure drops sharply (form S/C = 0 to S/C = 0.29) then decreases slightly. In the trailing edge region, the surface pressure increases slightly. This pressure distribution at the trailing edge easily leads to separation of the boundary-layers. The difference between the numerical and the experimental results is very small, which proves that the numerical method is reliable in the flow field prediction.

In fig. 8, the effect of turbulence models on turbine vane surface HTC shows significant difference. Standard k-ε model overestimates the HTC over the entire surface of the vane.

This is because standard k-ε model assumes that Reynolds stress is isotropic. The constitutive equation of k-ε model is:

$$-\overline{u}_i\overline{u}_j = \nu_t\left(\frac{\partial U_i}{\partial x_j}+\frac{\partial U_j}{\partial x_i}\right)-(2/3)k\delta_{ij} \tag{11}$$

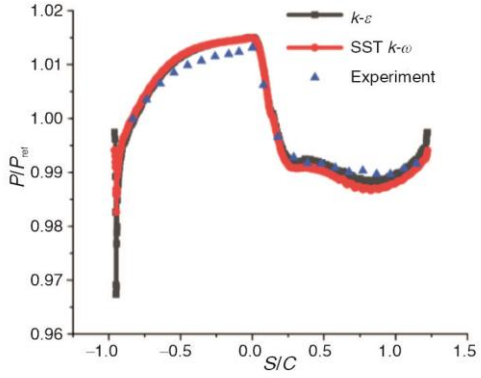

Figure 7. Surface pressure comparison between experimental and CHT simulation results

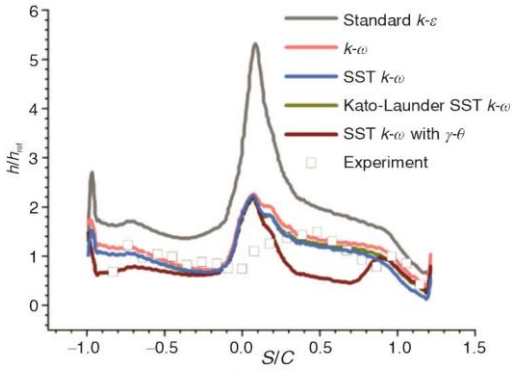

Figure 8. Surface HTC comparison between experimental and CHT simulation results

However, in turbine leading edge region, Reynolds stress is anisotropic. When flow is mainly dominated by normal stress, eq. (11) would cause large error. In leading edge region, eq. (11) overestimates turbulent kinetic energy generation. The process of transporting turbulent kinetic energy downstream would lead to overestimation of the convective HTC on the entire turbine surface. In [16], the phenomenon of excessively high turbulent kinetic energy generation at the stagnation point of the leading edge is called *stagnation point anomaly*. By comparison, the k-ω, SST k-ω, and Kato-Launder SST k-ω models show great agreement with experimental results. Only in stagnation region, all the three models overestimate HTC values. The maximal error for SST k-ω model is 147% at point S/C = 0.0. This difference is mainly because the direction of heat conduction is not 1-D around stagnation point result in measurement error of heat flux sensor. Although the Kato-Launder SST k-ω model uses limiter factor, it does not significantly improve the prediction accuracy in stagnation region. In the simulation, we should also consider the simulation time. The SST k-ω with Kato-Launder limiter factor consume more computer time, but it does not significantly improve the simulation accuracy. The SST k-ω with γ-θ transition model underestimates HTC values on pressure surface. On suction surface, it shows less accuracy between $0.3 < S/C < 0.7$ than other models. The γ-θ transition model underestimates heat transfer before transition point and this problem should be studied in next research. Through the previous analysis of comparisons, we decided to use SST k-ω model for the next analysis.

To further verify the accuracy of the simulation method, we conduct a comparative study with noted C3X experimental results [23]. The C3X turbine vane was cooled by 10 internal cooling holes. Figure 9 shows its simulation domain and grid division. The CHT method and SST k-ω turbulence model are used in simulation. The comparison between the simulation results and the experimental results are shown in fig. 10. The simulation results agree well with the experimental results both in terms of value and variation trend. In fig. 10(c),

there is slight difference around point *S/C* = 0.25. This is mainly because complex flow structure in transition section. The previous analysis indicates that the numerical simulation method used in this paper satisfies the requirements of subsequent studies.

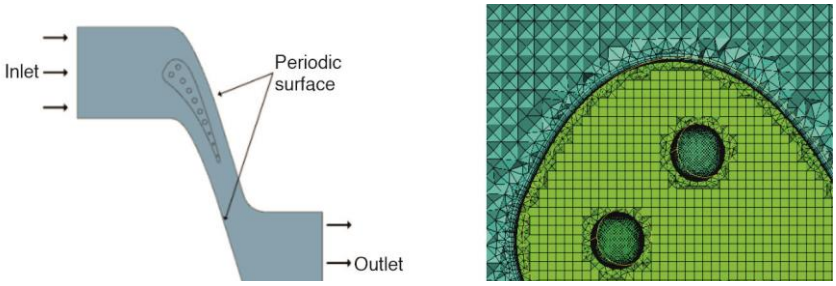

Figure 9. The C3X turbine vane computational domain and grid division (a) Computational domain and (b) Grid division

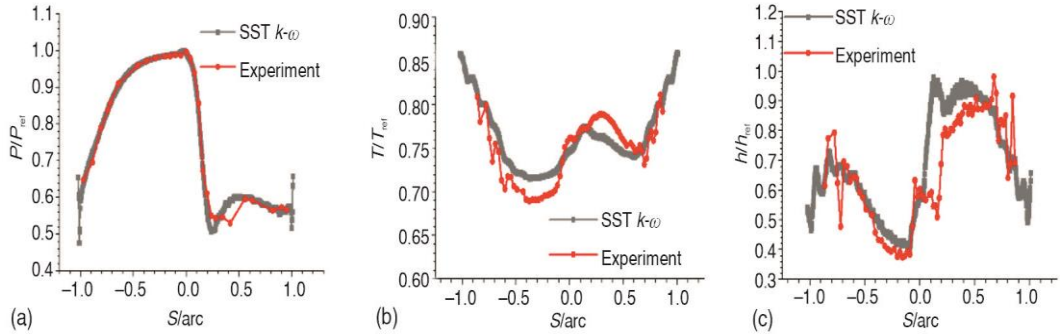

Figure 10. Comparison between experimental and CHT simulation results at middle plane of C3X vane; (a) pressure distributions, b) temperature distributions, and (c) HTC distributions

Conclusion

In this paper, the simulation method is validated by experimental results firstly. In experiment, a real-sized turbine guide vane model and corresponding test wind tunnel are designed. A thin film heat flux sensor is used to measure the heat flux on the turbine surface. Compared with the previous measurement methods, the heat flux sensor can measure heat flux directly, reducing the measurement error of indirect investigation. The design and installation method of the experimental instruments are described in detail in this paper, which could be used as references for other experimental design. In numerical simulation, the fluid and solid temperature fields are solved by using CHT method. In addition, we have verified the simulation accuracy of different turbulence models coupling with transition model and limiter factor in CHT method. The results indicate that the SST model shows better accuracy and economy than other models studied in this paper for heat transfer prediction.

References

[1] Boyce, M. P., *Gas Turbine Engineering Handbook*, Elsevier, Amsterdam, The Netherlands, 2011
[2] Koop, W., The Integrated High Performance Turbine Engine Technology (IHPTET) Program, https://ntrs.nasa.gov/citations/19890016803

[3] Hennecke, D., *Turbine Blade Cooling in Aeroengines*, Von Karman Institute Lecture Series, Sint-Genesins-Rode, Belgium, 1982
[4] Nealy, D., *et al*., Measurements of Heat Transfer Distribution over the Surfaces of Highly Loaded Turbine Nozzle Guide Vanes, *Journal of Engineering Gas Turbines Power*, *106* (1984), 1, pp. 149-158
[5] Arts, T., *et al*., Aerothermal Performance Measurements and Analysis of a Two-Dimensional High Turning Rotor Blade, *Journal of Turbomachinery*, *120* (1998), 3, pp. 494-499
[6] Graziani, R., *et al*., An Experimental Study of Endwall and Airfoil Surface Heat Transfer in a Large Scale Turbine Blade Cascade, *Journal of Engineering Power*, *102* (1980), 2, pp. 257-267
[7] Lang, H., *et al*., Stereoscopic Particle Image Velocimetry in a Transonic Turbine Stage, *Experiments in Fluids*, *32* (2002), 6, pp. 700-709
[8] Giess, P., *et al*., Detailed Experimental Survey of the Transonic Flow Field in a Rotating Annular Turbine Cascade, *Proceedings*, 2nd European Conference on Turbomachinery-Fluid Dynamics and Thermodynamics, Antwerpen, Belgium, 1997
[9] Giel, P., *et al*., Blade Heat Transfer Measurements and Predictions in a Transonic Turbine Cascade, *Proceedings*, ASME 1999 International Gas Turbine and Aeroengine Congress and Exhibition, Indianapolis, Ind., USA, 1999
[10] Ganzert, W., *et al*., An Experimental Study on the Aerodynamics and the Heat Transfer of a Suction Side Film Cooled Large Scale Turbine Cascade, *Proceedings*, ASME 1999 International Gas Turbine and Aeroengine Congress and Exhibition, Indianapolis, Ind., USA, 1999
[11] Buck, F. A., *et al*., Design and Evaluation of a Single Passage Test Model to Obtain Turbine Airfoil Film Cooling Effectiveness Data, *Proceedings*, ASME 1995 International Gas Turbine and Aeroengine Congress and Exhibition, Houston, Tex., USA, 1995
[12] Radomsky, R.W., *et al*., Flowfield Measurements for a Highly Turbulent Flow in a Stator Vane Passage, *Journal of Turbomachinery*, *122* (2000), 2, pp. 255-262
[13] Kodzwa Jr, P. M., Measurements of Film Cooling Performance in a Transonic Single Passage Model, Ph. D. thesis, Stanford University, Stanford, Cal., USA, 2005
[14] Laskowski, G., *et al*., Inverse Design of and Experimental Measurements in a Double-Passage Transonic Turbine Cascade Model, *Journal of Turbomachinery*, *127* (2005), 3, pp. 619-626
[15] Facchini, B., *et al*. Conjugate Heat Transfer Simulation of a Radially Cooled Gas Turbine Vane, *Proceedings*, ASME Turbo Expo 2004: Power for Land, Sea, and Air, Vienna, Austria, 2004
[16] Luo, J., *et al*., Conjugate Heat Transfer Analysis of a Cooled Turbine Vane Using the V2F Turbulence Model, *Journal of Turbomachinery*, *129* (2007), 4, pp. 773-781
[17] Walker, G., The Role of Laminar-Turbulent Transition in Gas Turbine Engines: A Discussion, *Journal of Turbomachinery*, *11* (1993), 2, pp. 207-216
[18] Medic, G., *et al*., Toward Improved Prediction of Heat Transfer on Turbine Blades, *Journal of Turbomachinery*, *124* (2002), 2, pp. 187-192
[19] Taulbee, D. B., Tran, L., Stagnation Streamline Turbulence, *AIAA Journal*, *26* (1988), 8, pp. 1011-1013
[20] Menter, F. R., *et al*., A Correlation-Based Transition Model Using Local Variables—Part I: Model Formulation, *Journal of Turbomachinery, 128* (2006), 3, pp. 413-422
[21] Langtry, R. B., *et al*., Correlation-Based Transition Modeling for Unstructured Parallelized Computational Fluid Dynamics Codes, *AIAA journal*, *47* (2009), 12, pp. 2894-2906
[22] Kato, M., The Modelling of Turbulent Flow Around Stationary and Vibrating Square Cylinders, *Turbulent Shear Flow, 1* (1993), Jan., pp. 10.4. 1-10.4. 6
[23] Hylton, L., *et al*., Analytical and Experimental Evaluation of The Heat Transfer Distribution Over the Surfaces of Turbine Vanes, Final Report Detroit Diesel Allison, NASA, Washington DC, 1983
[24] Kline, S. J., Describing Uncertainty in Single Sample Experiments, *Mechanical Engineering, 75* (1953), Jan., pp. 3-8

Paper submitted: August 20, 2021
Paper revised: December 17, 2021
Paper accepted: January 24, 2022